A safe and sustainable bacterial cellulose nanofiber separator for lithium rechargeable batteries

Hyeokjo Gwon[a,1], Kitae Park[b,1], Soon-Chun Chung[c,1], Ryoung-Hee Kim[a], Jin Kyu Kang[b], Sang Min Ji[a], Nag-Jong Kim[c], Sunghaeng Lee[c], Jun-Hwan Ku[a], Eun Cheol Do[d], Sujin Park[c], Minsang Kim[d], Woo Yong Shim[c], Hong Soon Rhee[c], Jae-Young Kim[c], Jieun Kim[c], Tae Yong Kim[c], Yoshitaka Yamaguchi[e], Ryo Iwamuro[e], Shunsuke Saito[e], Gahee Kim[d], In-Sun Jung[d], Hyokeun Park[d], Chanhee Lee[d], Seungyeon Lee[d], Woo Sung Jeon[d], Woo Dae Jang[f], Hyun Uk Kim[f], Sang Yup Lee[f], Dongmin Im[a], Seok-Gwang Doo[d], Sang Yoon Lee[d], Hyun Chul Lee[b,2], and Jin Hwan Park[c,2]

[a]Next Generation Battery Lab, Material Research Center, Samsung Advanced Institute of Technology, Samsung Electronics Co., Ltd., Yeongtong-gu, Suwon-si, Gyeonggi-do 16678, Republic of Korea; [b]Samsung Particulate Matter Research Institute, Samsung Advanced Institute of Technology, Samsung Electronics Co., Ltd., Yeongtong-gu, Suwon-si, Gyeonggi-do 16678, Republic of Korea; [c]Biomaterials Lab, Material Research Center, Samsung Advanced Institute of Technology, Samsung Electronics Co., Ltd., Yeongtong-gu, Suwon-si, Gyeonggi-do 16678, Republic of Korea; [d]Samsung Advanced Institute of Technology, Samsung Electronics Co., Ltd., Yeongtong-gu, Suwon-si, Gyeonggi-do 16678, Republic of Korea; [e]Samsung R&D Institute Japan, Samsung Electronics Co., Ltd., Yokohama 230-0027, Japan; and [f]Metabolic and Biomolecular Engineering National Research Laboratory, Department of Chemical and Biomolecular Engineering (BK21 Plus Program), Institute for the BioCentury, Korea Advanced Institute of Science and Technology, Daejeon 34141, Republic of Korea

Edited by Yi Cui, Stanford University, Stanford, CA, and accepted by Editorial Board Member Richard Eisenberg August 14, 2019 (received for review April 2, 2019)

Bacterial cellulose nanofiber (BCNF) with high thermal stability produced by an ecofriendly process has emerged as a promising solution to realize safe and sustainable materials in the large-scale battery. However, an understanding of the actual thermal behavior of the BCNF in the full-cell battery has been lacking, and the yield is still limited for commercialization. Here, we report the entire process of BCNF production and battery manufacture. We systematically constructed a strain with the highest yield (31.5%) by increasing metabolic flux and improved safety by introducing a Lewis base to overcome thermochemical degradation in the battery. This report will open ways of exploiting the BCNF as a "single-layer" separator, a good alternative to the existing chemical-derived one, and thus can greatly contribute to solving the environmental and safety issues.

bacterial cellulose | lithium batteries | cellulose separator | gene engineering

Safety and environmental issues associated with the large-scale battery are becoming a major public concern (1–3). A separator is one of the most crucial components of a battery that is closely related with these aspects (4). Recently, cellulose materials have received tremendous attention as an alternative to the polyolefin-based separators, owing to their high thermal stability and excellent electrolyte wettability as well as natural abundance (5–13). The separator in a lithium ion battery (LIB) should facilitate fast Li ion transport in the liquid electrolyte. Therefore, it should have a porous structure for ion transfer as well as excellent mechanical strength and thermal stability. Bacterial cellulose nanofiber (BCNF) membrane is highly porous, hydrophilic, and has a 3D network structure cross-linked with hydrogen bonding between the hydroxyl groups of cellulose nanofiber; as a result, pure BCNF shows superior physicochemical properties such as high tensile strength and high thermal stability (*SI Appendix*, Fig. S1). Although they have been extensively investigated in energy applications (14–17), the studies on their use as separators are limited to small-scale batteries, and they reportedly show an intrinsically low thermal shrinkage rate (7–9). Moreover, the yield of BCNF is still limited for successful commercialization (18).

Here, we report the development and in-depth characterization of the battery full cell composed of the entire process of BCNF production, including the genetic modification of the strain, mass fermentation, and large-area membrane preparation, and its integration into a battery via the roll-to-roll manufacture process. We demonstrate battery full cell with the BCNF separator showing remarkable cycle stability with 80% capacity retention even after 1,000 cycles that is available for commercial use (19, 20). Furthermore, we present the highest BCNF yield per glucose (31.5%) reported so far, by increasing the metabolic flux toward BCNF formation. Notably, we found that the high thermal stability of the BCNF is not fully implemented in a full-cell battery. It was identified that the structure of BCNF is thermochemically degraded by acidic gases produced by the decomposition of the lithium salt $LiPF_6$, used in the battery. This issue was overcome by including a Lewis base such as polyethylene glycol (PEG) to maintain the structure and improve the safety of the battery.

Fig. 1*A* schematizes the preparation of BCNFs and manufacture of an 18650 LIB, which is cylindrical battery with a diameter of 18 mm and a length of 65 mm. Wild-type bacterial strains, *Komagataeibacter xylinus* DSM 2325 (Koma), which produce cellulose nanofibers (CNFs), were obtained from the Leibniz Institute DSMZ (German Collection of Microorganisms and Cell Cultures).

Significance

This report describes an opportunity for the bacterial cellulose nanofiber (BCNF) membrane, which has recently been attracting much attention due to its sustainability and high thermal stability, as a "single-layer," good alternative membrane to the existing chemical-derived one in batteries, and thus allows us to find possible solutions to the environmental and safety issues. We achieved highest BCNF yield ever reported so far and fabricated a cylindrical lithium ion battery (LIB) by roll-to-roll process to realize remarkable cycle stability with 80% capacity retention even after 1,000 cycles, which is comparable to those of commercialized batteries. Finally, we introduced a Lewis base to improve thermal safety of the battery to a level comparable to that of a commercial ceramic-coated separator.

Author contributions: H.G., J.K.K., D.I., S.-G.D., Sang Yoon Lee, H.C.L., and J.H.P. designed research; H.G., K.P., S.-C.C., R.-H.K., J.K.K., S.M.J., N.-J.K., S.L., J.-H.K., E.C.D., S.P., M.K., W.Y.S., H.S.R., J.-Y.K., J.K., T.Y.K., Y.Y., R.I., S.S., G.K., I.-S.J., H.P., C.L., S.L., W.S.J., W.D.J., H.U.K., and Sang Yup Lee performed research; H.G., N.-J.K., J.-H.K., T.Y.K., G.K., I.-S.J., H.P., C.L., S.L., H.U.K., Sang Yup Lee, D.I., and S.-G.D. analyzed data; and H.G., K.P., S.-C.C., H.C.L., and J.H.P. wrote the paper.

The authors declare no conflict of interest.

This article is a PNAS Direct Submission. Y.C. is a guest editor invited by the Editorial Board.

[1]H.G., K.P., and S.-C.C. contributed equally to this work.

[2]To whom correspondence may be addressed. Email: hc001.lee@samsung.com or jh111.park@samsung.com.

This article contains supporting information online at www.pnas.org/lookup/suppl/doi:10.1073/pnas.1905527116/-/DCSupplemental.

First published September 9, 2019.

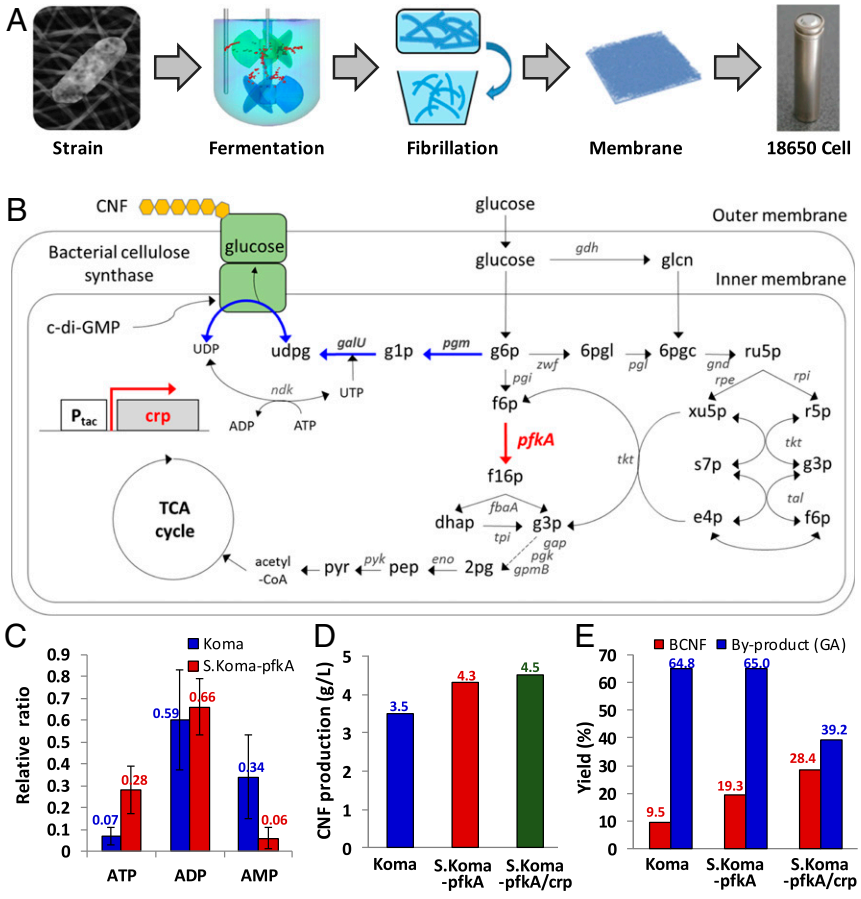

Fig. 1. Overall process for cellulose nanofiber (CNF) production and battery manufacture, and the metabolic engineering of a CNF-producing strain. (*A*) Overall scheme for the construction of a bacterial CNF membrane for battery separators. (*B*) Schematic representation of the CNF production pathway in a metabolically engineered strain (S.Koma-pfkA/crp). The blue lines represent the CNF biosynthesis pathway from glucose 6-phosphate. The bold red arrows indicate the heterologous expression of *pfkA* and *crp* gene under the control of the tac promoter. Details for the construction of plasmids, abbreviations of genes and metabolites, and the primers used for gene modification are available in *SI Appendix*, Tables S1 and S2. (*C*) Intracellular adenosine triphosphate (ATP), adenosine diphosphate (ADP), and adenosine monophosphate (AMP) ratio in wild-type Koma and S.Koma-pfkA strains. The error bar represents the SD of 3 measurements. (*D*) CNF production and (*E*) yield of Koma, S.Koma-pfkA, and S.Koma-pfkA/crp, respectively. The yield of the by-product, gluconic acid (GA), is also shown in *E*.

After constructing a metabolically modified strain, we produced large quantities of BCNF using a series of 30-L fermenters. The BCNF was further fibrillated for disentanglement and homogenization using a high-pressure homogenizer. Subsequently, a thin membrane was prepared by adding propylene carbonate as a pore-making agent and carboxymethylcellulose (CMC) to control the air permeability. Finally, we successfully manufactured a cylindrical battery via a continuous roll-to-roll process (Fig. 1*A*).

BCNF is produced through energy metabolism in a bacterial strain, with glucose as the carbon source. Furthermore, with genome sequencing and analysis, we reconstructed a genome-scale metabolic network of Koma (Fig. 1*B*). Particularly, glucose-6-phosphate (g6p) dehydrogenase (G6PD), which is sensitive to adenosine triphosphate (ATP) and associated with nicotinamide adenine dinucleotide (NAD), is a key branch-point for increasing the CNF yield (21–23). When ATP levels increase, the activity of G6PD is inhibited, and thus, the metabolic flux enters g6p to produce CNF. Glucose metabolism is the main energy source of ATP production. Interestingly, in most of the CNF-producing bacteria, glucose is metabolized through the oxidative pentose phosphate pathway and not the Embden–Meyerhof–Parnas (EMP) pathway, because of a lack of the *pfkA* gene, which is encoded with phosphofructokinase (24–26). The absence of the *pfkA* gene is a very well-known genotypic feature of the *Komagataeibacter* species, but the gene expression effect has not been studied well until now. Through simulated flux balance analysis with an additional reaction catalyzed by *pfkA* gene, we found that the expression of the *pfkA* gene is more beneficial for both the CNF production rate and specific growth rate (*SI Appendix*, Fig. S2). This could be because of the production of additional moles of ATP through the intact glycolysis upon the expression of the *pfkA* gene. The simulations suggest that using *Komagataeibacter* mutant with the *pfkA* gene expressed as a base production strain could be advantageous for further engineering of the process to optimize the CNF production. Thus, we introduced the *Escherichia coli pfkA* gene into the Koma (S.Koma-pfkA) to increase the intracellular ATP level (Fig. 1*C* and *SI Appendix*, Fig. S3*A*), thus achieving enhanced production and yield of CNF (Fig. 1 *D* and *E*). These results suggest that the recovery of the EMP pathway is important for enhancing the BCNF production and yield. To further increase the metabolic flux of EMP pathway, several genes (*pgi*, *pgk*, *fba*, *tpi*, *gap*, *gpm*, *pck*, and *mae*) were constitutively expressed in S.Koma-pfkA under the control of the tac promoter. However, the production and yield of BCNF did not increase significantly. Previously, Deng et al. (27) reported that the cAMP receptor protein (*crp*) deletion mutant does not produce any CNFs and regulates the expression of other genes involved in the cellulose biosynthesis. The CRP, a major global regulator in *E. coli* controlling the transcription initiation of genes, is mainly involved in the catabolism of alternate carbon sources and central carbon metabolism (28). Moreover, the CRP

positively regulates the expression of *fba*, *glk*, *pck*, and *pgi* genes in *E. coli*. Thus, we constructed the S.Koma-pfkA/crp strain under the control of the tac promoter (*SI Appendix*, *Methods* and Tables S1–S5). Compared with Koma, the S.Koma-pfkA/crp strain showed increased cellulose production (~1.3 times higher from 3.5 to 4.5 g/L) and a high increase in yield (~3 times higher from 9.5 to 28.4%) (Fig. 1 *D* and *E*). Surprisingly, the S.Koma-pfkA/crp strain showed a sharp decrease in the yield of gluconic acid (GA) (from 64.8 to 39.2%), which is the main by-product in the production of BCNF (Fig. 1*E*). These results suggest that CRP plays a role in regulating the multiple gene expression, not only EMP pathway-related genes to produce BCNF, but also glucose dehydrogenase (*gdh*) gene to prevent by-product.

In this study, we have constructed the genome-scale metabolic network and identified that introduction of *pfkA* gene is a critical point for improving the CNF yield. Previous studies were shown that the addition of ethanol results in a metabolic flux of *g6p* to CNF biosynthesis through the inhibition of G6PD enzyme activity by the increased levels of ATP (22, 23). Our simulation results shows that *pfkA* gene is not only increased the ATP flux-sum to 35.45 mmol/grams dry cell weight (gDCW)/h from 19.16 mmol/gDCW/h, but also central metabolic fluxes, such as glucose-6-phosphate isomerase (*pgi*), fructose bisphosphate aldolase (*fba*), triosephosphate isomerase (*tpi*), glyceraldehyde 3-phosphate dehydrogenase (*gap*), and enolase (*eno*). However, overexpression of these genes was not significantly beneficial to production of CNF and yield for glucose in Koma. Interestingly, S.Koma-pfkA strain only enhanced the intracellular ATP level, thus achieving improved production and yield of BCNF (Fig. 1 *C*–*E*). It suggests that the reaction to fructose-1,6-phosphate from fructose-6-phosphate by phosphofructokinase (*pfk*) is irreversible step in EMP pathway. Although S.Koma-pfkA strain still produced the high yield of GA (65%), these observations suggest that recovery of EMP pathway through *pfkA* gene may contribute to the energy metabolism for production of BCNF. To fully elucidate the effect of *pfkA* gene, further studies are underway.

To optimize the fermentation process, we used computational fluid dynamics (CFD) (*Materials and Methods*) to predict the turbulent energy (TE) and shear stress (SS) for various impeller types (Rushton, pitch-blade), agitation speeds (50 to 350 rpm), and viscosities (1 to 40 cP) (Fig. 2*A*). By optimizing the impeller configuration (pitch-type, 60°, blade number 2), we obtained higher TE/SS ratio and mass transfer coefficient (k_La), which increased the dissolved oxygen content (Fig. 2*B*). We further optimized the process with a higher dried cell mass (0.96 g/L at pH 5.0) from a high seed cell process (*SI Appendix*, Fig. S3*B*) and optimal oxygen composition (25%). Thus, for the S.Koma-pfkA/crp, with these optimized conditions (pitch-type-60°-blade impeller 2; seed pH, 5.0; 25% oxygen), we finally achieved higher BCNF productivity than wild-type Koma (from 0.16 to 0.29 gBCNF/L/h). In addition, we obtained the highest BCNF yield reported so far (from 9.5 to 31.5% gBCNF per g glucose) (Fig. 2*C* and *SI Appendix*, Fig. S3*C* and Table S6). It is necessary to further improve the BCNF's productivity and minimize the accumulation of the GA in the industrial aspects, although our study exhibited advanced results compared to the previous. The continuous process is considered as the promising strategy compared to the batch fermentation. Main barriers in the continuous fermentation are Koma cell-based genetic instability due to long-term shear stress exposure and CNF aggregation. Currently, further studies are being conducted for optimized CNF continuous fermentation process to solve the related problems. Finally, we successfully mass-produced BCNF using a series of 30-L fermentation reactors using the optimized conditions (*SI Appendix*, Fig. S4).

We fabricated 15-μm-thick BCNF nonwoven membranes, consisting of stacked layers with a small diameter of 21.5 ± 12 nm on

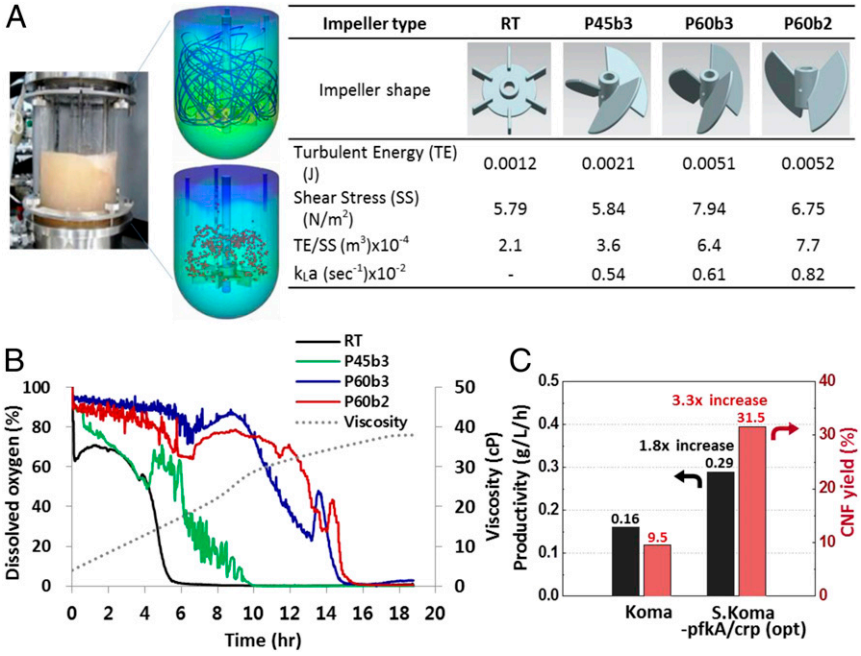

Fig. 2. CFD for optimizing the fermentation process. (*A*) Three-dimensional fluid models for turbulent energy and sheer stress using various impeller types: RT (Rushton type), P45b3 (pitch type, 45°, blade #3), P60b3 (pitch type, 60°, blade #3), P60b2 (pitch type, 60°, blade #2) at 10 cP, 250 rpm. k_La (volumetric oxygen transfer coefficient) = $\ln(\Delta DO)/(\Delta t)$ (DO, dissolved oxygen) at 40 cP, 250 rpm. The pitch-type impellers showed much higher turbulent energy with higher shear stress than those in the Rushton-type impeller. The P60b2 impeller showed highest TE/SS and k_La. (*B*) Dissolved oxygen vs. time; increasing the dissolved oxygen by optimizing the impeller configuration. The viscosity gradually increases over time, and in the case of RT, DO decreased rapidly after 6 h. The pitch-type impeller with 2 blades (P60b2) exhibited the highest dissolved oxygen amount as a function of time. (*C*) Plot demonstrating the improved CNF productivity and yield of the optimized strain, S.Koma-pfkA/crp (opt). The optimized S.Koma-pfkA/crp showed much higher CNF productivity (0.29 gCNF/L/h), which is 1.8 times higher, and CNF yield (31.5%), which is 3.3 times higher than wild-type Koma strain.

average, with many open pores and investigated their properties (Fig. 3 *A* and *B* and *SI Appendix*, Fig. S1*A*). Then, we successfully fabricated a large-area BCNF separator that can be applied in a continuous roll-to-roll process for producing a cylindrical battery (Fig. 3*C*). The properties of separator were optimized with tensile strength of ∼60 MPa and air permeability of 200 s/100 cm^{-3}, which is sufficient for commercial use (4). Moreover, BCNF separator exhibited high wettability and thermal resistivity compared to commercial polyolefin and ceramic-coated separators (CCSs) (*SI Appendix*, Fig. S1 *B*–*E*). We confirmed that the BCNF can tolerate severe thermal stress up to 338 °C via thermomechanical analysis (TMA) (Fig. 3*D*). Moreover, the BCNF membrane does not shrink and maintains its shape at 300 °C; in contrast, the CCS shrunk at 160 °C and the deformation began in a fixed frame (Fig. 3*D*, *Inset*). Therefore, in order to verify how those superior properties of BCNF affect the electrochemical performance in the actual battery, we evaluated the full cell battery performance. The cylindrical 18650 battery (500 mA·h) with the BCNF separator showed remarkably better cycle performance than the commercial CCS (Fig. 3*E*); it retained 80% of the initial capacity even after 1,000 cycles, which implies that it is comparable for commercial batteries (19, 20). The relative direct current–internal resistance (DC-IR) increase ratios of the BCNF battery increased by 9% after 300 cycles, which is comparable to that of the CCS battery (Fig. 3*E*, *Inset*). The superior electrochemical performance of the BCNF battery is presumably owing to its cross-linked 3D network structure, which leads to high porosity, high crystallinity, low membrane resistance, and excellent electrolyte wettability.

After confirming the excellent battery performance of BCNF, in order to find out whether the high thermal stability of the

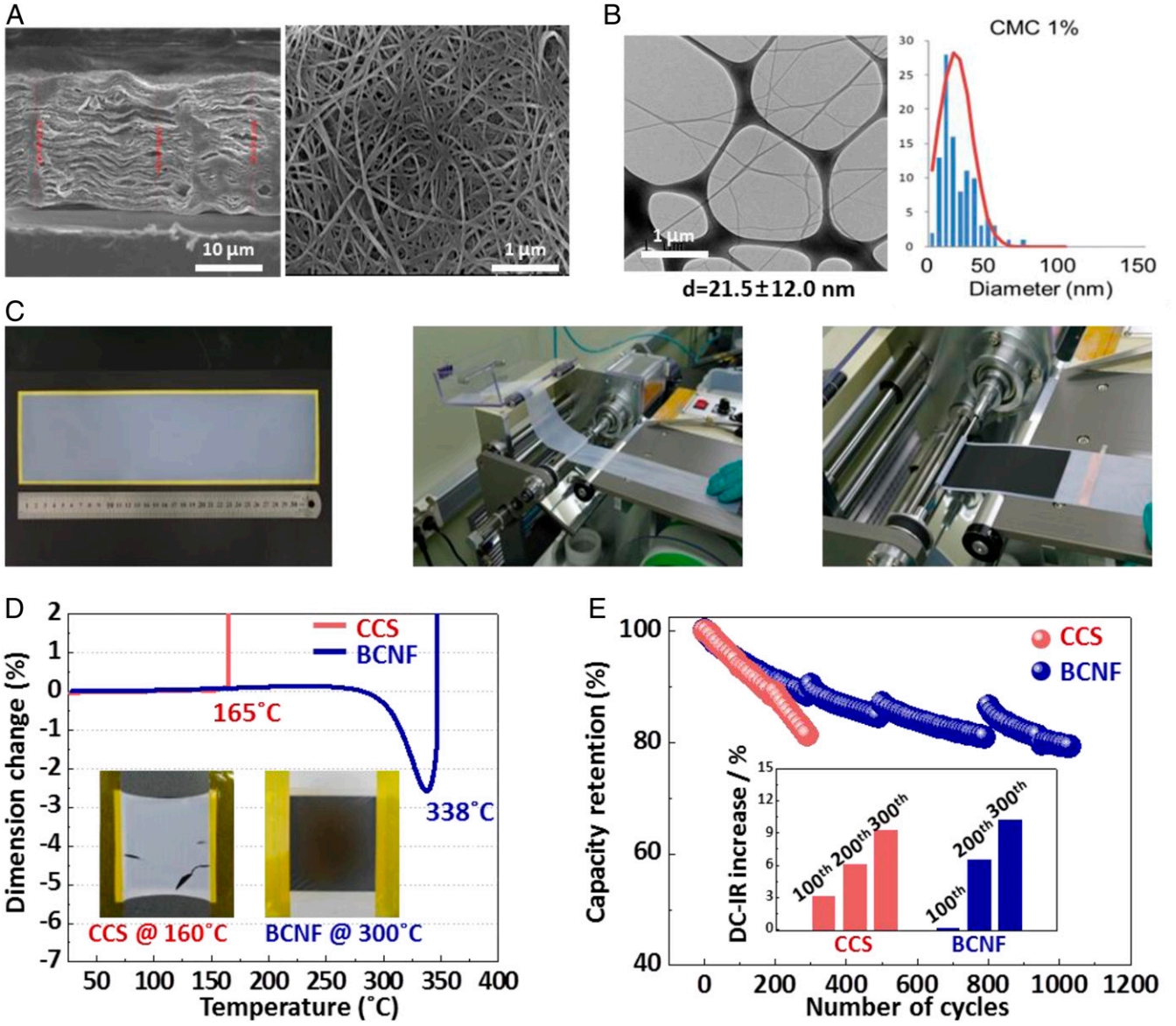

Fig. 3. BCNF membrane and battery performances. (*A*) Side view (*Left*) and top view (*Right*) scanning electron microscopy (SEM) of the BCNF membrane. (*B*) Transmission electron microscopy (TEM) and distribution of the diameter of BCNF produced with 1% carboxymethylcellulose (CMC). (*C*) Large-area BCNF membrane and manufacture of a cylindrical LIB full cell via the roll-to-roll process. (*D*) Thermomechanical analysis (TMA) of the ceramic-coated separator (CCS) and BCNF separator. The BCNF exhibited much higher thermal tolerance up to 338 °C compared than that of 165 °C of the CCS. The *Inset* shows the thermal resistivity in a fixed frame at 160 °C (CCS) and 300 °C (BCNF), respectively. (*E*) Life cycle performances of CCS and BCNF in 18650 battery full cells. The *Inset* shows the relative direct current–internal resistance (DC-IR) increase ratios after every 100 cycles at 25 °C.

BCNF is implemented in the actual full cell, we first investigated the thermal behavior of the BCNF separator via the hot-box test under rather harsh conditions at 170 °C. Consequently, the BCNF separator, even as a single-layer membrane, showed higher thermal stability than a commercial polyolefin separator (Fig. 4*A*). However, in order to clarify the reason why the excellent thermal stability of the BCNF (*SI Appendix*, Fig. S1 *D* and *E*) is not fully implemented in the full cell battery, we further investigated the effect of the actual battery environment on the BCNF membrane. X-ray photoelectron spectroscopy analysis revealed many LiF, C–F_x, P–O, and C–O species on the surface of BCNF after heat exposure (*SI Appendix*, Fig. S5), which implies that chemicals, including F species, are deposited on the surface. A battery contains various chemical components such as electrodes, binders, conducting agents, and electrolytes. Such a chemical environment might cause complex chemical reactions with the BCNF, and thus significantly affect its safety performance. Among various battery components, an electrolyte containing lithium salts and carbonate-based solvents is the most likely candidate that can react with the BCNFs because of its relatively high chemical reactivity. We performed differential scanning calorimetry to find that each of the carbonate solvents such as ethylene carbonate (EC), ethyl methyl carbonate (EMC), dimethyl carbonate (DMC), and vinylene carbonate (VC) reacts with the BCNF at a relatively high temperature (>280 °C) (*SI Appendix*, Fig. S6*A*). In contrast, in the presence of lithium hexafluorophosphate ($LiPF_6$), an exothermic reaction occurred below 200 °C (*SI Appendix*, Fig. S6*B*). Interestingly, *ex situ* hot-box test with heat exposure (170 °C for 1 h) revealed that the BCNF is carbonized to a dark material at high temperatures, with significant deterioration of its mechanical strength, only when an electrolyte containing $LiPF_6$ was used (Fig. 4 *B*–*D*). We observed various anions such as F^-, PF_6^-, and PO_4^{3-} on the carbonized BCNF (*SI Appendix*, Fig. S6*C*). Moreover, the crystallinity of the BCNF decreased (11) and the Fourier-transform infrared (FTIR) intensity of the C–O bonds caused by the decomposition of the cellulose structure increased as the temperature increased from 25 to 170 °C (*SI Appendix*, Fig. S6 *D* and *E*), implying that the BCNF could pyrolyse into levoglucosenone much more easily at higher temperatures (*SI Appendix*, Fig. S6 *F* and *G*).

It is well known that $LiPF_6$ decomposes into strong Lewis acids, such as LiF and PF_5, at elevated temperatures that could chemically attack the BCNF (29, 30). Therefore, to reduce the effect of

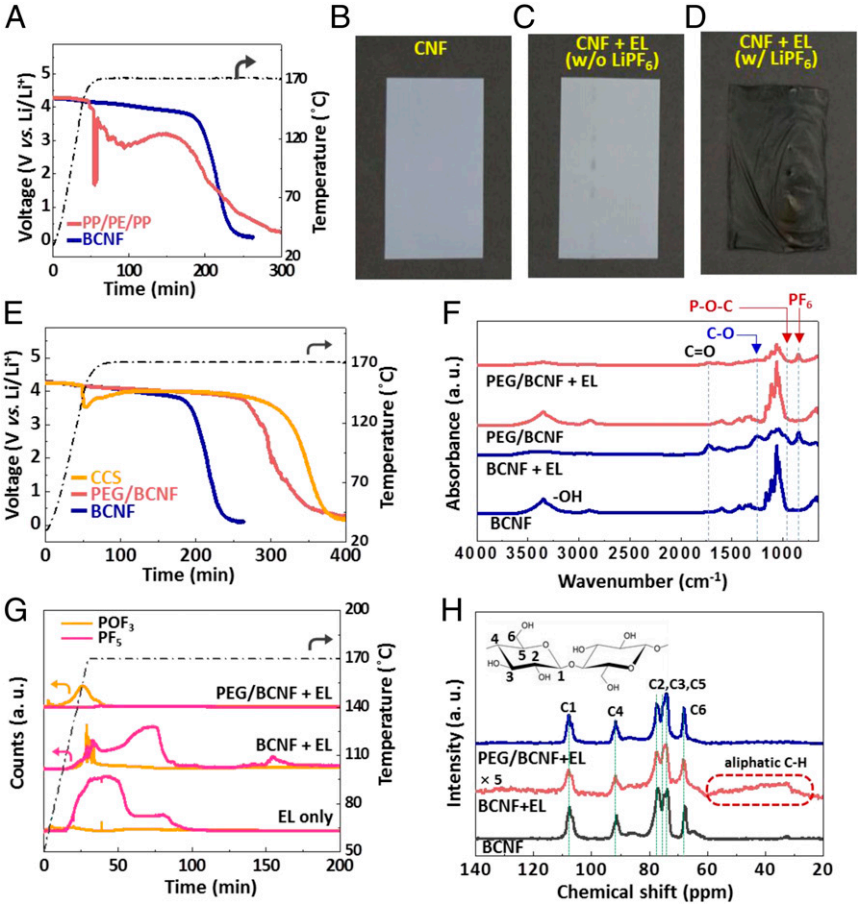

Fig. 4. Thermal safety performances and characterization of BCNF. (*A*) Thermal safety performance of BCNF and polypropylene/polyethylene/polypropylene (PP/PE/PP) (purchased from Celgard). (*B*) Photographs showing the carbonization of BCNF at 170 °C. (*C*) BCNF with the electrolyte (EL) (without $LiPF_6$) at 170 °C. (*D*) BCNF with the EL (including $LiPF_6$) at 170 °C. The BCNF is carbonized only in the presence of $LiPF_6$. (*E*) Thermal safety performance of BCNF, enhanced thermal safety of PEG/BCNF, and ceramic-coated separator (CCS) (purchased from Toray) in the hot-box test. (*F*) Fourier-transform infrared (FTIR) spectra of BCNF and PEG/BCNF, heat-treated at 170 °C. The C–O, P–O–C, and PF_6 peaks in FTIR on the carbonized BCNF decreased on the PEG/BCNF. (*G*) Evolved gas analysis (EGA) of the EL, BCNF + EL, and PEG/BCNF + EL, respectively. The total amount of evolved gas was drastically reduced on the PEG/BCNF. (*H*) Solid-state ^{13}C CP-MAS NMR spectra of heat-treated BCNF, BCNF + EL, and PEG/BCNF + EL at 170 °C. The BCNF showed typical peaks of cellulose, viz., distinguishable chemical shifts corresponding to the 6 carbon atoms in cellulose, according to their different bonding. However, these characteristic NMR signals decreased sharply and peaks related to C–H appeared simultaneously, when BCNF was heat-treated with an electrolyte containing $LiPF_6$, implying that it transformed to aliphatic chain forms owing to structural degradation. In contrast, the PEG/BCNF shows NMR peaks in keeping with the structural characteristics of cellulose.

these Lewis acids, we introduced a Lewis base such as PEG to maintain the cellulose structure and enhance the thermal stability of the battery. Indeed, the carbonization of BCNF could be mitigated by introducing PEG into the electrolyte (*SI Appendix*, Fig. S7*A*). Therefore, we intended to insert PEG directly into the BCNF (*SI Appendix*, Fig. S7 *B* and *C*). Consequently, we demonstrated the improved thermal safety of the battery in full-cell level (Fig. 4*E*). This implies that the outstanding safety performance, which is comparable to that of commercialized CCS, can be obtained by the BCNF membrane as a "single-layer" separator system without any support layers.

We confirmed the disappearance of the C–C bond at 1,580 cm^{-1} through Raman spectroscopy (*SI Appendix*, Fig. S7*D*), and the structural deterioration of the BCNF was also mitigated (*SI Appendix*, Fig. S7*E*). FTIR spectral analysis confirmed a drastic decrease in the intensity of the C–O peak owing to the collapse of the cellulose structure (Fig. 4*F*). Interestingly, there was no PF_5 gas generation upon the introduction of PEG, whereas POF_3 and PF_5 gases were generated when only BCNF was used (Fig. 4*G*). In the ^{13}C cross-polarization/magic angle spinning (CP/MAS) NMR spectrum (Fig. 4*H*), the BCNF containing PEG shows NMR peaks with the structural characteristics of cellulose maintained, which is mainly attributed to the effective reduction of the Lewis acids in the presence of PEG. Based on our findings, we could further improve thermal safety of BCNF through further safety-enhancing research, and thus the BCNF membrane could be an outperforming next-generation separator for sustainability, thermal safety, and battery performance.

In summary, we presented the entire process for the production of sustainable BCNF and battery manufacturing. A maximum BCNF yield was achieved through the genetic manipulation of the strain and optimal fermentation based on the understanding of their complex metabolic flux system. We demonstrated a large-capacity battery, showing superior cycle life compared to the commercialized battery, by installing a large-scale fermentation reactor and fabrication of a uniform large-area BCNF membrane using CFD and pore-forming controls. In particular, we improved their safety performance by introducing a Lewis base such as PEG to maintain the CNF structure, based on the identification of the BCNF's degradation mechanism through the thermochemical reaction with the electrolyte component in the actual battery system. The results obtained in this study suggest that the BCNF membrane, which has intrinsically high thermal stability, can be a promising alternative to the chemical-derived membrane, as a sustainable safety-enhanced separator for the next generation of batteries.

Materials and Methods

Details of bacterial culture, construction of plasmids, genome sequencing of Koma, and construction of metabolically engineered strains and plasmids appear in *SI Appendix*. CFD method, fermentation procedure, preparation and characterization of the BCNF separator, 18650 cell preparation, and electrochemical analysis are also in *SI Appendix*.

ACKNOWLEDGMENTS. This work was supported by the Samsung Electronics Co., Ltd. We thank Sungwoo Hwang from Samsung Advanced Institute of Technology, Samsung Electronics Co., Ltd., for his valuable comments and discussion.

1. M. Armand, J. M. Tarascon, Building better batteries. *Nature* **451**, 652–657 (2008).
2. D. Larcher, J. M. Tarascon, Towards greener and more sustainable batteries for electrical energy storage. *Nat. Chem.* **7**, 19–29 (2015).
3. J. Zhang *et al.*, Renewable and superior thermal-resistant cellulose-based composite nonwoven as lithium-ion battery separator. *ACS Appl. Mater. Interfaces* **5**, 128–134 (2013).
4. P. Arora, Z. J. Zhang, Battery separators. *Chem. Rev.* **104**, 4419–4462 (2004).
5. M. Iguchi, S. Yamanaka, A. Budhiono, Bacterial cellulose—a masterpiece of nature's arts. *J. Mater. Sci.* **35**, 261–270 (2000).
6. F. Esa, S. M. Tasirin, N. A. Rahman, Overview of bacterial cellulose production and application. *Agric. Agric. Sci. Procedia* **2**, 113–119 (2014).
7. Q. Xu *et al.*, A bacterial cellulose/Al_2O_3 nanofibrous composite membrane for a lithium-ion battery separator. *Cellulose* **24**, 1889–1899 (2017).
8. F. Jiang, L. Yin, Q. Yu, C. Zhong, J. Zhang, Bacterial cellulose nanofibrous membrane as thermal stable separator for lithium-ion batteries. *J. Power Sources* **279**, 21–27 (2015).
9. W. Xiao, J. Liu, C. Yan, Nanofiber/ZrO_2-based mixed matrix separator for high safety/high-rate lithium–ion batteries. *Chem. Phys. Lett.* **686**, 134–139 (2017).
10. R. J. Moon, A. Martini, J. Nairn, J. Simonsen, J. Youngblood, Cellulose nanomaterials review: Structure, properties and nanocomposites. *Chem. Soc. Rev.* **40**, 3941–3994 (2011).
11. M. Poletto, H. L. Ornaghi, A. J. Zattera, Native cellulose: Structure, characterization and thermal properties. *Materials (Basel)* **7**, 6105–6119 (2014).
12. J. Zhang *et al.*, Sustainable, heat-resistant and flame-retardant cellulose-based composite separator for high-performance lithium ion battery. *Sci. Rep.* **4**, 3935 (2014).
13. J.-H. Kim *et al.*, Functionalized nanocellulose-integrated heterolayered nanomats toward smart battery separators. *Nano Lett.* **16**, 5533–5541 (2016).
14. Y. Ko *et al.*, Flexible supercapacitor electrodes based on real metal-like cellulose papers. *Nat. Commun.* **8**, 536 (2017).
15. J. Song *et al.*, Processing bulk natural wood into a high-performance structural material. *Nature* **554**, 224–228 (2018).
16. S. Wang *et al.*, Transparent, anisotropic biofilm with aligned bacterial cellulose nanofibers. *Adv. Funct. Mater.* **28**, 1707491 (2018).
17. S. Galland *et al.*, Cellulose nanofibers decorated with magnetic nanoparticles—synthesis, structure and use in magnetized high toughness membranes for a prototype loudspeaker. *J. Mater. Chem. C* **1**, 7963–7972 (2013).
18. J. W. Hwang, Y. K. Yang, J. K. Hwang, Y. R. Pyun, Y. S. Kim, Effects of pH and dissolved oxygen on cellulose production by *Acetobacter xylinum* BRC5 in agitated culture. *J. Biosci. Bioeng.* **88**, 183–188 (1999).
19. G. Mulder *et al.*, Comparison of commercial battery cells in relation to material properties. *Electrochim. Acta* **87**, 473–488 (2013).
20. N. Nitta, F. Wu, J. T. Lee, G. Yushin, Li-ion battery materials: Present and future. *Mater. Today* **18**, 252–264 (2015).
21. P. Ross, R. Mayer, M. Benziman, Cellulose biosynthesis and function in bacteria. *Microbiol. Rev.* **55**, 35–58 (1991).
22. T. Naritomi, T. Kouda, H. Yano, F. Yoshinaga, Effect of ethanol on bacterial cellulose production from fructose in continuous culture. *J. Ferment. Bioeng.* **85**, 598–603 (1998).
23. S. Yunoki, Y. Osada, H. Kono, M. Takai, Role of ethanol in improvement of bacterial cellulose production: Analysis using ^{13}C-labeled carbon sources. *Food Sci. Technol. Res.* **10**, 307–313 (2004).
24. H. Zhang *et al.*, Complete genome sequence of the cellulose-producing strain *Komagataeibacter nataicola* RZS01. *Sci. Rep.* **7**, 4431 (2017).
25. C. Prust *et al.*, Complete genome sequence of the acetic acid bacterium *Gluconobacter oxydans*. *Nat. Biotechnol.* **23**, 195–200 (2005).
26. K. Illeghems, L. De Vuyst, S. Weckx, Complete genome sequence and comparative analysis of *Acetobacter pasteurianus* 386B, a strain well-adapted to the cocoa bean fermentation ecosystem. *BMC Genomics* **14**, 526 (2013).
27. Y. Deng, N. Nagachar, C. Xiao, M. Tien, T. H. Kao, Identification and characterization of non-cellulose-producing mutants of *Gluconacetobacter hansenii* generated by Tn5 transposon mutagenesis. *J. Bacteriol.* **195**, 5072–5083 (2013).
28. T. Shimada, N. Fujita, K. Yamamoto, A. Ishihama, Novel roles of cAMP receptor protein (CRP) in regulation of transport and metabolism of carbon sources. *PLoS One* **6**, e20081 (2011).
29. H. Yang, G. V. Zhuang, P. N. Ross, Jr, Thermal stability of $LiPF_6$ salt and Li-ion battery electrolytes containing $LiPF_6$. *J. Power Sources* **161**, 573–579 (2006).
30. S. Lux *et al.*, The mechanism of HF formation in $LiPF_6$ based organic carbonate electrolytes. *Electrochem. Commun.* **14**, 47–50 (2012).